**Shaina Riaz**
Interdisciplinary Research Center for Refining & Advanced Chemicals (IRC-RAC) King Fahd University of Petroleum & Minerals, Dhahran, Saudi Arabia

**Saad Kamran**
Ex-student, Mechanical Engineering Department, King Fahd University of Petroleum & Minerals (KFUPM), Dhahran Saudi Arabia

**Masoud A-Rasheidi**
Interdisciplinary Research Center for Sustainable Energy Systems (IRC-SES) King Fahd University of Petroleum & Minerals (KFUPM), Dhahran, Saudi Arabia

**Mohamed E. Zayed**
Interdisciplinary Research Center for Sustainable Energy Systems (IRC-SES) King Fahd University of Petroleum & Minerals (KFUPM), Dhahran, Saudi Arabia

**Shafiqur Rehman**
Interdisciplinary Research Center for Sustainable Energy Systems (IRC-SES) King Fahd University of Petroleum & Minerals (KFUPM), Dhahran, Saudi Arabia

**Firoz Khan**
Interdisciplinary Research Center for Sustainable Energy Systems (IRC-SES) King Fahd University of Petroleum & Minerals (KFUPM), Dhahran, Saudi Arabia

# Structural and Optical Band Gap Engineering of Cu–Li Co-Doped NiO Nanostructures for Optoelectronic and Energy Applications

*This study presents Cu- and Li-co-doped nickel oxide (NiO) nanostructures that exhibit significant improvements in structural and optical properties. NiO samples, including pure, singly doped, and co-doped versions, are synthesized using the hydrothermal method. The structural, optical, and morphological characteristics are analyzed through X-ray diffraction (XRD), UV–visible spectroscopy, and scanning electron microscopy (SEM). XRD results revealed enhanced crystallinity in NiO films due to dual doping, making these materials promising for microelectronics applications. Refractive index and absorption coefficient demonstrated improvements in NiO with both single and co-doping. The band gap energy decreased from 3.50 eV for Cu-doped NiO to 3.34 eV for Cu, Li co-doped films. This reduction in band gap suggests that Cu and Li co-doping significantly enhances the electrochromic performance of the NiO samples. The increased absorbance in the NCL7 sample underscores the potential for fine-tuning dopant levels to further improve performance.*

***Keywords:*** *Metal oxudes; Li co-doped NiO nano-films; Cu co-doped NiO films; Refractive index*

## 1. INTRODUCTION

Oxide electronics encompasses a wide array of materials and devices, including dielectrics, ferroelectrics, piezoelectrics, epitaxial oxides, memory devices, and sensors. Metal oxide (MO) semiconductors fundamentally differ from traditional inorganic semiconductors, such as silicon and III–V compounds, in terms of material design strategies, electronic structure and interactions, charge transport and transfer mechanisms, defect chemistry, thin-film fabrication techniques, and optoelectronic properties [1]. These characteristics facilitate both the implementation of existing device functionality and the creation of wholly new apps [2]. The MOs can function as semiconductors, metals, or insulators, depending on their crystal structure and chemical composition. Their behavior can be tailored to be either n-type or p-type through doping. MO semiconductors, which support equilibrium populations of electrons and holes, are widely used in batteries, solar energy conversion, and display technologie [3], [4].
The discovery of hydrogenated amorphous silicon (a-Si) and organic semiconductors opened new possibilities in thin-film transistors. However, its relatively low carrier mobility (around 0.5–1.0 $cm^2\ V^{-1}\ s^{-1}$), lack of optical transparency, limited current-carrying capability, and moderate mechanical flexibility pose significant challenges to its use in future technologies [5].

Transport mechanisms in MOs are very different from those in silicon semiconductors, where hybridized $sp^3$ σ-bonding and $sp^3$ σ*-anti-bonding states characterize the conduction band minimum and valence band maximum. In the metal oxides examined in this study, the valence band is primarily constituted by occupied oxygen 2p antibonding states. In contrast, the conduction band predominantly derives from unoccupied metal ns bonding orbitals. The spherical symmetry of the ns orbitals around the conduction band minimum results in low electron effective masses in these oxides, hence facilitating efficient electron transport even in the amorphous phase [6]. This phenomenon originates from the effective overlap of spherically symmetric metal s orbitals, which is largely insensitive to lattice distortions, unlike the strongly directional $sp^3$ σ orbitals in silicon that undergo pronounced mobility degradation in the amorphous phase. Consequently, amorphous oxide se–miconductors (AOSs) often exhibit electron mobilities comparable to those of their crystalline counterparts. Moreover, the distribution of sub-bandgap density of states significantly

Received: June 2026, Accepted: July 2026
Correspondence to: Dr. Shafiqur Rehman,
King Fahd University of Petroleum & Minerals, Dhahran, Saudi Arabia,
E-mail: srehman@kfupm.edu.sa
**doi: 10.5937/fme2604600S**
© Faculty of Mechanical Engineering, Belgrade. All rights reserved

varies between amorphous covalent semiconductors. The sub-bandgap density of states in amorphous indium–gallium–zinc oxide is generally one to two orders of magnitude lower than that seen in a-Si [7].

To address these issues, researchers have focused on MOs, which offer distinct advantages over crystalline Si and other III–V semiconductors. MOs demonstrate excep–tional carrier mobilities, even in their amorphous forms, and are highly tolerant to mechanical stresses [8]. They are compatible with organic dielectric and photoactive substances and provide excellent optical transparency. More–over, high-quality metal oxide thin films appropriate for electronic applications can be produced by vapor- and solution-phase techniques under near-ambient conditions (about 25°C). These attributes make MOs beneficial for high-value applications, including cost-effective circuits, flexible organic light-emitting diode (OLED) screens, and solar systems built on plastic substrates [9].

Transparent semiconducting oxide thin films are highly sought after due to their outstanding optical pro–perties, extraordinary stability, and excellent electrical performance [10]. These transparent conducting oxides, fundamentally MO semiconductor materials, can be classified as either n-type or p-type. The demand for tran–sparent, conductive thin-film coatings of p-type semi–conductors in various optoelectronic applications is inc–reasing. Transparent semiconducting oxide thin films are ideal materials for sustainable buildings and renewable energy systems due to their high transparency, electrical conductivity, and long-term durability. Their use in energy-efficient smart windows, transparent photovol–taics, and wind turbine blade coatings helps to improve energy efficiency and system performance, and boost the lifetime of the system [11,12]. Nickel oxide (NiO), the most extensively studied p-type transition-metal oxide, is a promising material for several usages. These function as positive electrodes in batteries, solar-thermal absorbers, electrochromic displays, hetero–junction solar cells, and gas sensors [13,14]. NiO is recognized for its wide band gap, low cost, and ex–cellent cyclic stability, making it a promising material for ion storage [15].

In recent years, a significant number of studies have focused on tuning the electrochemical properties of NiO thin films by doping them with phosphorus [16], cobalt [17], aluminum [18], magnesium [19], lithium [20], indium [21], and others, employing various doping techniques. Multiple researches have indicated that co-doped NiO films, created using diverse fabrication techniques, demonstrate superior electrochromic performance relative to conventional monodoped NiO. For instance, Castro et al. [20] studied the structural properties of gradient Ni- and Mn-doped lithium cobalt oxide thin films produced by magnetron sputtering for lithium-ion batteries. The LMNCO thin films showed a clear compositional gradient throughout their thickness. Compared to virgin LCO, both LNCO and LMNCO showed significant redox activity, with LMNCO exhibiting superior Li-ion intercalation behavior and improved Mn redox performance. Hosseinzade et. al. [21] investigated the structural and electrochemical properties of Cu-doped NiO nanostructures using elec–trochemical impedance spectroscopy. The optimized NiO nanostructure containing 3% Cu exhibited mar–kedly improved performance, characterized by an app–ropriate bandgap of approximately 3.38 eV, enhanced electrical conductivity (0.04 mS $cm^{-1}$), a larger elec–troactive surface area (1.430 $cm^2$), and superior charge carrier mobility (1.36 $cm^2$ $V^{-1}$ $s^{-1}$). The structural pro–perties of Li doped NiO films grown on FTO substrates through spin coating technique were irradiated using 60 MeV Si ions under swift heavy ion radiation (SHIR) [22].

It was reported that the effect of SHIR had a positive influence on the structural properties of Li:NiO films, as well as the intensities of the first-order (1LO) and second-order (2LO) Raman modes were found to decrease following Si ion irradiation, indicating the formation of irradiation-induced defects. Huang et al. [23] examined Li-Ti co-doped NiO films synthesized by the sol-gel spin coating method, revealing a notable optical fluctuation of over 56% at 580 nm. Similarly, Lin et al. [24] developed Li-Zr-NiO films using radio-frequency magnetron sputtering, achieved optimal opti–cal modulations of 40% and 68% at 670 nm, res–pectively. Gillaspie et al. [25] also utilized radio-freq–uency magnetron sputtering to fabricate Li-W co-doped NiO films, which exhibited an optimal optical modu–lation of around 58%.

Chen et al. [26] explored Li-Cu co-doped NiO films fabricated via a chemical solution deposition technique. This co-doping approach significantly improved the transmittance and conductivity, highlighting the poten–tial of Li-Cu co-doped NiO films as p-type transparent conducting oxides. In another study, Uzunbayır et al. [27] synthesized Li, Cu-$NiO_x$ particles using the sol-gel method, maintaining a fixed Li content of 0.05 while varying the Cu content from 0 to 0.30. The authors found that incorporating Li+ and Cu2+ into the structure decreased both emission intensity and average decay time. Zhang et al. [28] documented the effect of lithium doping on the optoelectronic and transport properties of nickel oxide films. The films were produced using pulsed-laser deposition. The researchers noted that Li doping significantly improved the p-type conductivity of NiO; however, the room-temperature mobilities re–mained low across all films (<0.05 $cm^2$ $V^{-1}$ $s^{-1}$). X-ray photoemission and O K-edge absorption spectroscopy revealed a shift of the Fermi level towards the maxi–mum valence-band (MVB) and the formation of a new hole state due to Li doping.

The MVB and hole states predominantly consist of Zhang-Rice bound states, which account for the limited mobility [29]. Bhatt et al. [30] synthesized Li-doped NiO films using microwave synthesis and conducted first-principles simulations. Optical studies showed that the band gap of pure NiO decreased from 3.3 eV to 3.17 eV upon 1% Li doping. Additionally, the Li-doped NiO films exhibited increased electrical capacity and improved cyclability. Electrochemical impedance spectroscopy results indicated that the reversibility and conductance of Li-doped NiO films were significantly enhanced.

Chang et al. [31] examined Li-doped NiO electro–chromic films fabricated using RF magnetron sput–tering. Their findings indicate that Li doping markedly improves the performance of electrochromic devices by

augmenting charge storage capacity. The improved electrochromic device attained an intercalation charge of 11.93 mC/cm², an optical density variation of 0.38, a transmittance modulation of 44.1%, and a coloring efficiency of 31.8 cm²/C at 550 nm under 3.2 V.

Although earlier research has shown that Li- and Cu-doped NiO materials can enhance the optical, structural, and electrochemical performance of NiO-based thin films, most studies have concentrated on single-property enhancement or individual dopants, with little knowledge of the synergistic effects of Li–Cu co-doping. Mjority of existing studies focus on optical and structural characterization, with insufficient emphasis on the electrochemical mechanisms governing charge transfer and stability. Additionally, there is a lack of systematic optimization of dopant concentration and synthesis conditions to balance optical transparency and conductivity. Futher more, the long-term cycling dura–bility and environmental stability of Li–Cu co-doped NiO films have not been comprehensively assessed. To tackle these research gaps, this study explores the structural and optical properties of LixCu0.05 Ni0.95−xO nanocoatings with optimized Li concent–rations. It highlights the synergistic role of Li-Cu co-doping for advanced solar energy and optoelectronic applications.

This work introduces a new class of hybrid $Li_xCu_{0.05}Ni_{0.95-x}O$ nanocoatings engineered through controlled Li–Cu co-doping to simultaneously improve optical properties and visible-light transmittance, a combination not achieved in previous NiO-based studies. By opti–mizing Li content within a fixed Cu-doping framework, we reveal a synergistic electronic effect that modifies the band structure, enhances charge transport, and maximizes optical contrast relevant to solar applications. This integrated approach creates a new materials platform for high-performance solar and optoelectronic devices. This study used a hydrothermal method to prepare $Li_xCu_{0.05}Ni_{0.95-x}O$ (x = 0.0, 0.02, 0.05, 0.07) nanoparticles (NPs) with varying Li contents (0, 2, 5, and 7%).

Moreover, the investigation thoroughly analyzes the effect of Li inclusion on crystal structure, phase purity, crystallite size, defect deformation, and local elemental distribution, thereby explaining the structural aspects that determine material attributes. The outcomes anti–cipated that Li-Cu co-doping has a synergistic structural function in customizing the NiO lattice and enhancing the microstructure, which leads to improved optical behavior and charge transport.

## 2. EXPERIMENTAL PROTOCOLS AND MATERIALS

### 2.1 Synthesis of $Li_xCu_{0.05}Ni_{1-x}$ O Nanoparticles

$Ni(NO_3)_2.H_2O$, $Cu(NO_3)_2.3H_2O$, LiOH, and $NH_4OH$ were obtained from Sigma-Aldrich and used without further treatment. $Li_xCu_{0.05}Ni_{1-x}O$ nanoparticles (NPs) were synthesized using a hydrothermal method with varying stoichiometries, as outlined in Table 1. To begin, 0.035 mol of nickel nitrate hexahydrate ($Ni(NO_3)_2{\cdot}6H_2O$) was dissolved in 70 mL of deionized water (DW). Copper (II) nitrate trihydrate ($Cu(NO_3)_2 \cdot 3H_2O$) and lithium hydroxide (LiOH) were then added to the above solution at different molar ratios corres–ponding to $Li_xCu_{0.05}Ni_{0.95-x}O$ (where x = 0, 0.02, 0.05, and 0.07) while maintaining a constant copper content of 0.05 and adjusting the lithium content to 0, 2, 5, and 7%. A solution of ammonium hydroxide ($NH_4OH$) at a concentration of 0.1 mol in 100 mL of deionized water was incrementally added to achieve uniform distribution while stirring at ambient temperature. The reaction mixture was agitated for an extra hour at the same temperature. The formulated solution was introduced into a Teflon-lined stainless-steel autoclave and held at 180 °C for 8 hours to produce $Li_xCu_{0.05}Ni_{0.95-x}O$ nanoparticles. The nanoparticles were washed several times with deionized water and centrifuged at 10,000 rpm for 5 minutes. The samples were then dehydrated in a vacuum oven at 70°C overnight. The samples were subsequently annealed in air at 270°C for 2 hours, then dispersed in ethanol to a concentration of 10 mg/mL. Figure 1 illustrates the synthesis technique for $Li_xCu_{0.05}Ni_{0.95-x}O$ nanoparticles.

The previous studies, in the existing survey, showed that 5 mol % Cu provided an appropriate balance bet–ween enhanced electrical conductivity and improved optical absorption while preserving the single-phase NiO crystal structure. Therefore, in this study, 5 mol% Cu was chosen as a representative composition reported to provide structural stability while allowing the effect of Li concentration to be systematically investigated. All characterization devices were adjusted according to the manufacturers' recommended protocols before mea–surements were taken. The characterization techniques used demonstrated higher measurement accuracy and precision, ensuring the reliability and reproducibility of the derived structural, morphological, compositional, and optical properties. X-ray diffraction (XRD) assess–ments were conducted with an angular precision of ±0.02° (2θ). The field emission scanning electron mic–roscopy (FESEM) accelerating voltage was kept within the instrument tolerance of ±1%. The uncertainty in the EDS elemental composition analysis was roughly at ±1–2 wt.% for the elements analyzed. UV–Vis absorption spectra were obtained with a wavelength precision of ±0.5 nm. The photoluminescence (PL) spectra were collected with a wavelength precision of ±0.3 nm. The film thickness determined using spectroscopic ellipso–metry exhibited an uncertainty of roughly ±2–3 nm.

**Table 1. Sample codes and stoichiometry of $Li_xCu_{0.05}Ni_{0.95-x}O$ nanoparticles**

| Sample | Li | Cu | $Ni_{0.95-x}O$ |
|---|---|---|---|
| NC | 0 | 0.05 | 0.95 |
| NCL2 | 0.02 | 0.05 | 0.93 |
| NCL5 | 0.05 | 0.05 | 0.90 |
| NCL7 | 0.07 | 0.05 | 0.88 |

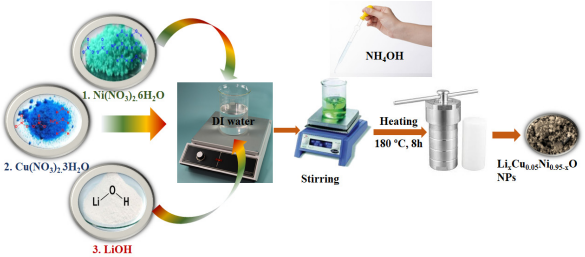



**Figure 1. Schematic diagram for the synthesis process of $Li_xCu_{0.05}Ni_{0.95-x}O$**

### 2.2 Characterization Techniques

The X-ray diffraction patterns of the prepared nano–particles were examined for phase identification using a Rigaku Miniflex-II system with Cu/Kα radiation (λ = 1.5406 Å). Fourier-transform infrared (FTIR) transmis–sion spectra were recorded using a Smart iTR NICOLET iS10 instrument to analyze the bonding cha–racteristics. The morphology and elemental composition of the prepared nanoparticles were characterized using scanning electron microscopy (SEM) and energy dispersive X-ray spectroscopy (EDS) with a JEOL SEM (Model: JSM6610LV). Absorption spectra, for all samples, were measured with a UV–Vis–NIR spectro–meter (JASCO, Model: UV-670). Ellipsometry measu–rements were conducted using a J.A. Woolam ellip–someter (Model: M-2000).

## 3. RESULTS AND DISCUSSION

### 3.1 XRD Analysis of $Li_xCu_{0.05}Ni_{0.95-x}$ Films

Figure 2a shows XRD patterns of NiO nanoparticles (NPs) with different Li concentrations and fixed Cu concentrations. The XRD patterns reveal five strong peaks that correspond to (111), (200), (220), (311), and (222) planes of the cubic NiO phase (JCPDS no.73–1523). No impurity phases were observed in the doped and undoped XRD spectra, indicating that Li and Cu atoms were incorporated into the NiO lattice without altering its cubic structure [32]. The most intense peak was the (200) plane, which implies a preferred orientation along this direction. No peaks, other than the NiO peaks, were observed, indicating that Li and Cu atoms may be incorporated into the NiO lattice [33].

Furthermore, it could be seen that the diffraction peaks were slightly shifted to lower angles upon inc–reasing the doping concentrations, suggesting that the doping process has increased the lattice constant of the NiO crystal [34]. Figure 2b illustrates the examination of the 2θ range of 43–44° to demonstrate the impact of additions on structural modifications. The Debye–Scherrer and Bragg equations were used to calculate the crystallite sizes and d-spacing [34]:

$$D = \frac{K\lambda}{\beta \cos\theta} \tag{1}$$

$$d = \frac{n\lambda}{2\sin\theta} \tag{2}$$

where K = 0.94 (Scherrer constant), λ = 1.5405 Å (wavelength of Cu Kα1 radiation), θ = diffraction angle of the peak, β = full width at half-maximum (FWHM) of the peak, n = 1 (order of reflection). The average crystallite size of nanoparticles markedly decreased with increasing lithium concentration. The determined grain sizes of nanoparticles were 8.092, 8.057, 8.042, and 8.026 nm for lithium concentrations of 0, 2, 5, and 7%, respectively. Table 2 shows the calculated full-width half maximum (FWHM), average crystallite size, and d-spacing of planes for all the prepared $Li_xCu_{0.05}Ni_{0.95-x}O$ Films.

### 3.2 FTIR of $Li_xCu_{0.05}Ni_{0.95-x}O$ Films

Figure 2c displays the FTIR spectra of all produced samples. The bands at 2933 $cm^{-1}$ and 1367 $cm^{-1}$ are attributed to the C-H stretching vibrations and O-C=O asymmetric stretching vibrations. Moreover, the absor–ption band appeared at 2344 $cm^{-1}$ is correspondent to the $CO_2$ molecules in the air [35]. The observed band at 3410 $cm^{-1}$ is associated with the O–H stretching vibrations of $H_2O$ molecules adsorbed by Li and Cu-doped NiO-NPs. The absorption band at ~1046 $cm^{-1}$ is assigned to different modes of Cu-O bending vibrations. In Figure 2d, the zoomed-in region (1900–700 $cm^{-1}$) provides a closer look at specific vibrational features [34]. The green-shaded region, located between 1700–1600 cm□¹, is assigned to the stretching vibration of the C=O group, which could be related to residual organic materials or solvents used during film preparation. The orange-shaded area between 1300-1400 is assigned to asymmetric stretching vibrations of the C=O group. Furthermore, the orange-highlighted area between 1000-1100 cm□¹ is associated with Cu-O stretching vibrations, indicating the successful incorporation of copper into the NiO lattice [36]. The slight variations in peak intensities across the spectra suggest differences in Li and Cu doping levels, influencing the vibrational cha–racteristics and bonding environments within the doped NiO structure.

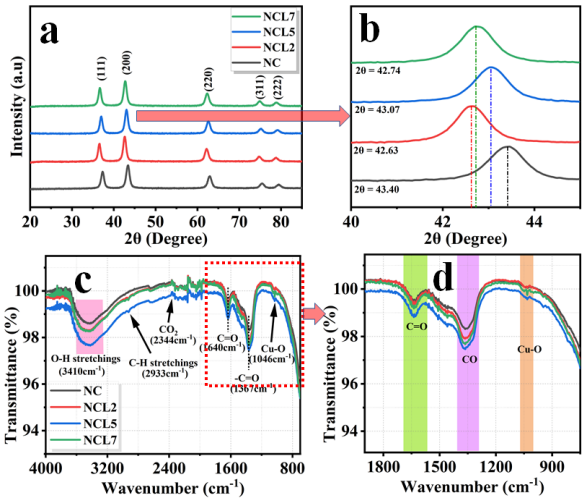



**Figure 2. (a, b) X-ray diffraction patterns and (c, d) FTIR Fourier-transform infrared transmission spectra of $Li_xCu_{0.05}Ni_{0.95-x}O$**

**Table 2. Structural calculations of $Li_xCu_{0.05}Ni_{0.95-x}O$ Films**

| Sample | Peak Position 2θ | FWHM β(°) | Crystallite size (D) (nm) | $d_{200}$ (nm) |
|---|---|---|---|---|
| NC | 43.4084 | 1.10349 | 8.092 | 0.284 |
| NCL2 | 42.6316 | 1.10541 | 8.057 | 0.283 |
| NCL5 | 43.074 | 1.10912 | 8.042 | 0.282 |
| NCL7 | 42.7409 | 1.11006 | 8.026 | 0.281 |

### 3.3 Morphology Analysis of $Li_xCu_{0.05}Ni_{0.95-x}O$ Films

Figure 3 illustrates the surface morphology of all produced samples. The SEM images demonstrate that the particles possess a porous architecture composed of nanoscale grains, indicating a well-dispersed structure.

The grains appear uniformly distributed, without any preferential orientation, a characteristic of the hydro–thermal synthesis technique. EDS mapping was con–ducted to further investigate the elemental composition, as shown in Figure 4. The mapping confirms a homogeneous distribution of key elements throughout the sample matrix, including Ni, O, and Cu. Due to EDS's technical limitations, it is common for Li to not appear in the elemental mapping even when it is present in the sample. The uniform distribution suggests that the doping process was successful and that no significant segregation or clustering of dopant atoms was observed. The presence of well-dispersed Ni, O, and Cu within the porous nanostructure may enhance the electronic and catalytic properties of the doped NiO films, making them suitable for various energy conversion and storage applications.

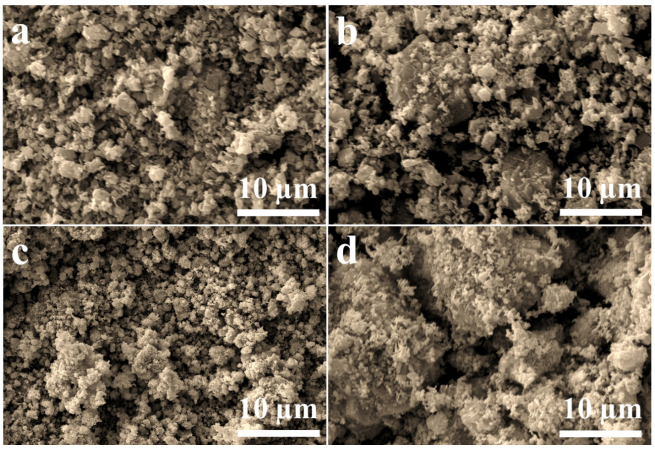



**Figure 3. Scanning electron microscopy images of LixCu0.05Ni0.95-xO for (a) x = 0%, (b) x = 2%, (c) x = 5%, and (d) x = 7%**

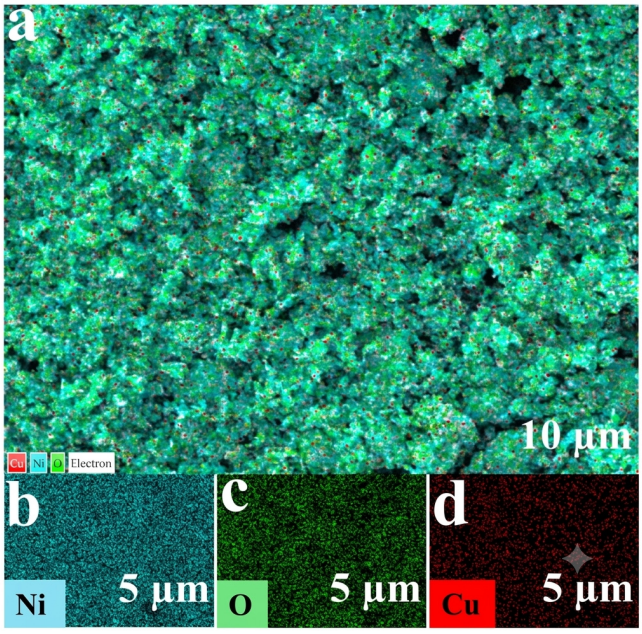



**Figure 4. Energy dispersive X-ray spectroscopy of $Li_xCu_{0.05}Ni_{0.95-x}O$ for x = 2% for (a) Mix, (b) Ni, (c) O, and (d) Cu**

Moreover, the SEM image revealeds a densely packed granular stracture composed of uniformly distri–buted fine particles with interconnected grains, indi–cating successful formation of the Cu- and Li-doped NiO structure without noticeable phase segregation. The corresponding EDS elemental mapping confirms a homogeneous distribution of Ni, O, and Cu throughout the sample, while the mixed elemental map demons–trates excellent compositional uniformity. The absence of Cu-rich agglomerates suggests that Cu is effectively incorporated into the NiO matrix, supporting the forma–tion of a chemically homogeneous doped oxide with high structural integrity.

### 3.4 UV-$V_{is}$ of $Li_xCu_{0.05}Ni_{0.95-x}O$ Films

UV-Vis spectroscopy was used to investigate the optical properties of NiOx films with varying Li concentrations. Figure 5a displays the optical absorbance spectra for Cu-doped NiO and Cu & Li co-doped thin films, spanning the wavelength range of 280 nm to 900 nm. The absorption profile demonstrates notable alterations in the optical characteristics of Li- and Cu-doped NiO films, as evidenced by a redshift of the absorption edges, a decrease in the band gap, and changes in the absorption coefficient. The findings indicate that co-doping with Cu and Li can effectively modulate the electrical and optical properties of NiO, making it a promising material for diverse applications, including photocatalysis, solar cells, and energy storage devices.

The higher absorbance of the NCL7 sample suggests the potential for tailored dopant concentrations to en–hance performance. The spectra show reduced absor–ption in the visible region, confirming that undoped NiO has minimal light absorption in this range. However, the doped samples, particularly NCL7, exhibit a notable increase in absorbance in the visible range. This could result from the introduction of Li and Cu ions, which create additional defect levels or states, thereby allo–wing the films to absorb more visible light.

The observed enhancement in visible-light absor–ption could significantly impact applications such as photocatalysis, where visible-light activation is desi–rable, underscoring the relevance of this research in the field. All samples show low absorption in the infrared region, with NCL7 again showing a slight increase. This slight increase in infrared absorbance could reflect dopant-related changes in the material's electronic structure, although it remains minimal compared to the UV and visible regions.

Figure 5b offered an enlarged view of the UV re–gion, providing further insight into the optical behavior of the Li and Cu-doped NiO films across different doping levels. In the UV region, a pronounced absor–ption peak is visible for all samples, consistent with the band-to-band electronic transitions in NiO. The absor–bance intensities vary among the samples, with NCL7 (green) showing the highest absorption, indicating en–hanced light harvesting due to increased dopant con–centrations. The broadening of the absorption peaks with increased doping, especially for the NCL7 sample, suggests a possible increase in defect states or changes in the crystal structure, which may create localized energy levels within the band gap. These novel findings will pique the interest of researchers in the solar and semiconductor fields.

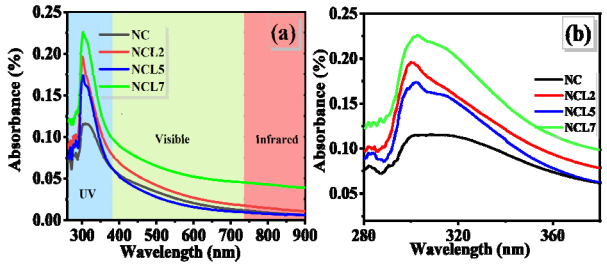



**Figure 5. Absorbance value of the dispersion solution of $Li_xCu_{0.05}Ni_{0.95-x}O$ NPs in a (a) wide range and (b) short range**

Figure 6a shows the absorption coefficient of $NiO_x$ films. The absorption coefficient values were reduced with the increase in Li content. As expected, the absorption coefficient decreased in the visible range for the doped samples relative to NC, aligning with the observed reduction in absorption in the UV-visible spectra. Higher doping levels, particularly in NCL7, cause a more pronounced decrease in the absorption coefficient, indicating changes in electronic transitions. However, the high absorption coefficient in the UV region persists across all samples, validating the material's ability to absorb UV light efficiently, although doping tunes this property. The optical direct bandgaps ($E_g$) of all the prepared NiOx films were determined from the absorbance data by Tauc plots (Figure 6b) as reported in Ref. [37];

$$\alpha h\nu = \beta(h\nu - E_g)^2 \tag{3}$$

Here, $h\nu$ and α denote the photon energy and the absorption coefficient, respectively, computed using the formula α=2.303A/t, where A represents absorbance and t signifies film thickness. The constant β denotes the band edge parameter.

Table 3 tabulates the obtained $E_g$ values for NC, NCL2, NCL5, and NCL7, respectively. The doped samples exhibited progressively lower band gaps as the doping concentration increased, with NCL7 having the smallest band gap. This result demonstrates that co-doping NiO with Cu and Li is an effective strategy to narrow the band gap, which could enhance its potential for applications such as photocatalysis or solar energy conversion.

**Table 3. Calculated bandgap of $Li_xCu_{0.05}Ni_{0.95-x}O$ Films**

| Sample | Band gap (eV) |
|---|---|
| NC | 3.50 |
| NCL2 | 3.45 |
| NCL5 | 3.35 |
| NCL7 | 3.34 |

Figure 6c presents the relationship between the absorption coefficient and the band gap with two y-axes. The absorption coefficients of specific wavelengths (1000, 800, 600, and 400 nm) for all samples (NC, NCL2, NCL5, and NCL7) are plotted on the primary y-axis. The corresponding band gaps for each sample are plotted on the secondary y-axis. This dual-axis plot helps visualize how Cu and Li doping levels simultaneously affect the optical absorption properties and the electronic band structure.

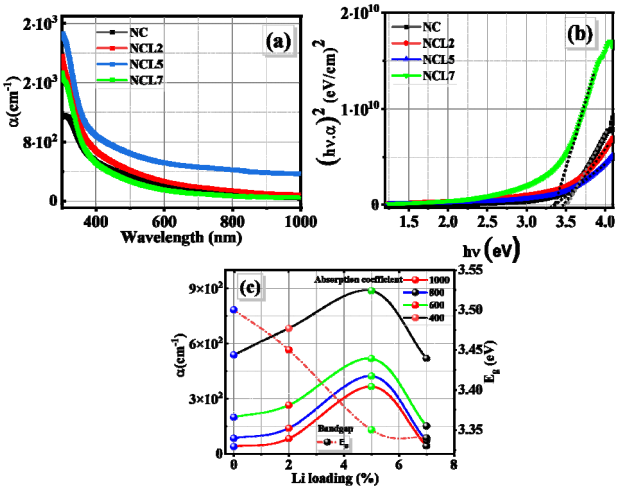



**Figure 6. (a) Absorption coefficient, (b) Tauc's plot, and (c) absorption coefficient with Li content of $Li_xCu_{0.05}Ni_{0.95-x}O$ films**

At higher wavelengths (1000 nm and 800 nm), the absorption coefficients for all samples are relatively low, indicating weak absorption in the infrared region, which is expected for NiO-based materials. However, as the wavelength decreases to 600 nm and 400 nm, an increase was observed in the absorption coefficient, especially for the undoped NC sample, which aligns with its larger band gap. The doped samples (NCL2, NCL5, and NCL7) exhibited progressively lower absorption coefficients at these wavelengths, indicating that doping reduces the material's ability to absorb light in this region due to band gap narrowing.

The secondary y-axis displays the corresponding band gaps for each sample, showing a clear decreasing trend with increased doping concentrations. NCL7 has the highest doping level and exhibits the smallest band gap. This decrease in the band gap correlates with the redshift in absorption seen in the UV-visible spectra (Figures 3a and b). The plot revealed a clear inverse relationship between the band gap and the absorption coefficient at lower wavelengths (400-600 nm), where the doped samples absorb less light as their band gap decreases. This combined analysis in Figure 4c demonstrates that increasing Cu and Li doping reduces the band gap and decreases the absorption coefficient at higher wavelengths. This behavior is consistent with that observed in Figure 3 and Figures 4a and b. The dual-axis plot clearly illustrates the tunability of the optical properties of NiO films via doping, making them suitable for applications requiring narrow band gaps and controlled absorption characteristics, such as photovoltaic and optoelectronic devices.

The absorption profile demonstrates notable alterations in the optical characteristics of Li- and Cu-doped NiO films, as evidenced by a redshift of the absorption edges, a decrease in the band gap, and changes in the absorption coefficient. The findings indicate that co-doping with Cu and Li can effectively modulate the electrical and optical properties of NiO, making it a promising material for diverse applications, including photocatalysis, solar cells, and energy storage devices. The elevated absorbance of the NCL7 sample suggests the potential for tailored dopant concentrations to enhance performance.

### 3.5 PLS of $Li_xCu_{0.05}Ni_{0.95-x}O$ Films

The structural modifications observed from XRD and the morphological evolution revealed by FESEM are expected to influence the electronic structure and defect density of the Cu–Li co-doped NiO nanostructures. Therefore, Photoluminescence spectroscopy (PLS) analysis was performed to investigate the effect of these structural changes on the radiative recombination behavior of charge carriers. PLS is a non-contact, non-destructive technique widely used to evaluate the optical quality of thin-film materials. In this method, the sample is irradiated with electromagnetic radiation of an appropriate wavelength, resulting in photon absorption and the promotion of charge carriers to higher-energy electronic states. As these excited electrons return to lower energy states, they recombine with photo-generated holes, emitting photons with slightly lower energy. Several factors, including the energy gap between the higher and lower states, the quality of the thin film, the nature of the dopant, and the presence of impurities and defect states, influence the energy of the emitted photons [38]. The PLS of undoped and Li, Cu, co-doped NiO NPs excited at 320 nm are shown in Figure 5a**.** The PL spectra of all the Li, Cu-co-doped NiO films showed four peaks at 365 nm, 407 nm, 434 nm, and 494 nm. The peak at approximately 365 nm presumably signifies near-band-edge emission in the ultraviolet range, typically ascribed to exciton recombination (bound electron-hole pairs) or transitions between shallow defect states adjacent to the conduction band edge.

In NiO, this emission may arise from intrinsic defects, such as oxygen vacancies or nickel interstitials, that generate defect levels near the conduction or valence band. The peak at 407 nm resulted from stock shift (certain defects) and band-to-band recombination, whereas the peak at 434 nm is likely due to near band edge emission triggered by exciton–exciton recombination [39].

The structure exhibits a significant defect density, as indicated by the emission peaks in the visible spectrum. The transitions responsible for the highest excitation at 320 nm involved the oxygen 2p states in the valence band and the nickel 3d levels in the conduction band. The emission band at 494 nm resulted from the recombination of electrons in the $Ni^{2+}$ vacancy with holes in the valence band. Doping with $Li^{+}$ and $Cu^{2+}$ decreased the photoluminescence emission intensity, indicating an increased recombination rate of photo-generated carriers in the NiO nanoparticles. The addition of $Li^{+}$ and $Cu^{2+}$ decreased the recombination rate [40]. The decrease in PL intensity highly depended on the crystallite size, as confirmed by XRD results. The decrease in PL intensity highly depended on the crystallite size, as confirmed by XRD results.

### 3.6 Refractive index of $Li_xCu_{0.05}Ni_{0.95-x}O$ Films

The refractive index (n) of a material is defined as the ratio of the speed of light in a vacuum to its phase velocity in the medium. Electromagnetic radiation, as it traverses a medium, experiences dispersion, scattering, attenuation, and absorption. Thus, the refractive index is more accurately defined as a complicated, frequency-dependent parameter that delineates both phase propagation and energy dissipation of the electro–magnetic wave as estimated in Ref. [41]:

$$n^* = n + ik \tag{4}$$

$$n = \left(\frac{1+R}{1-R}\right) + \sqrt{\frac{4R}{(1-R)^2} - k^2} \tag{5}$$

where R is the reflectance of the material and *k* is the extinction coefficient. The values of n and k, as a function of wavelength (λ) functions offer insights into the local field and electronic polarizability of ions, as depicted in Figures 6a and b, respectively. The Co-doped NiO samples demonstrated an enhanced ref–ractive index. The findings indicated that Cu and Li co-dopants contributed to a greater increase in refractive index than single doping due to the higher polarization of Cu and Li atoms within the NiO lattice structure [42].

Effective permittivity is concerned with mixtures when the inclusions are seen as a continuous random medium rather than as discrete. Dinulović and Rašuo [43] introduced an analytical technique for estimating the loss tangent and material dielectric constant for composite materials. In another study, they proposed an effective model for predicting the dielectric constant and loss tangent of epoxy composites reinforced with hollow ceramic spheres and E-glass fibers. The model showed better agreement with experimental at lower volume fractions of hollow ceramic spheres in the epoxy matrix [44].

To further validate the structural and optical modi–fications discussed in the previous sections, the optical constants were analyzed using spectroscopic ellip–sometry. Figure 6b illustrates that the k value for the pure NiO sample was the lowest, suggesting that the NiO host lattice contained minimal defects. As the do–ping concentration in the NiO sample increased, the k values also enhanced, reaching a maximum at x=0.05, which is attributed to an increase in defects within the host lattice.

Ellipsometry measurements were performed to determine the optical constants of the $Li_xCu_{0.05}Ni_{0.95-x}O$ films. The experimental data were fitted to models using the "CompleteEASE" software. A bi-layer system was employed for the modeling, and discrepancies were minimized using the Levenberg–Marquardt algorithm [45]. The real ($\varepsilon_1$) and imaginary ($\varepsilon_2$) parts of the die–lectric constant for the prepared samples were obtained from the following equations [45]:

$$\varepsilon 1 = n^2 - k^2 \tag{6}$$

$$\varepsilon 2 = 2nk \tag{7}$$

The fitted data for $\varepsilon_1$ and $\varepsilon_2$ as functions of wave–length are shown in Figures 7a and 7b, respectively. Initially, both $\varepsilon_1$ and $\varepsilon_2$ decrease rapidly for $\lambda < 380$ nm, then exhibit a slight decrease over the range of 370–1500 nm. These results indicate that co-doping enhances the optical response of the NiO film. As shown in Figure 7(a), $\varepsilon_1$ is high in the UV region and gradually stabilizes in the visible–NIR range, showing strong

electronic polarization from inter-band transitions. Doping with Cu and Li alters $\varepsilon_1$, with NCL7 displaying slightly lower values at longer wavelengths, suggesting reduced polarizability due to Li-induced lattice distor–tions. Figure 7(b) demonstrates that $\varepsilon_2$, which relates to dielectric losses, decreases sharply with wavelength; NCL2 and NCL5 have higher $\varepsilon_1$ in the UV region due to increased absorption from Cu–Li co-doping. NCL7's lower $\varepsilon_2$ indicates diminished optical losses, making it suitable for low-loss optoelectronic devices.

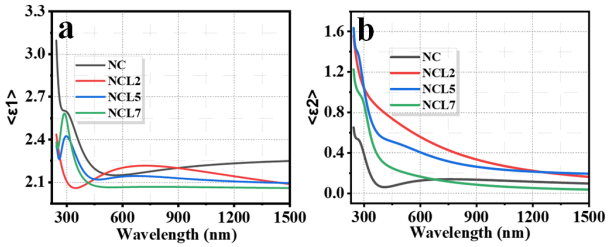



**Figure 7. (a) Epsilon (ε1) and (b) Epsilon (ε2) of LixCu0.05Ni 0.95-xO films**

Ellipsometric measurements (Figure 8) reveal that ψ remains high in the UV and stabilizes across the visible–NIR spectrum, with NCL7 showing increased ψ, indicating stronger light–matter interactions. Figure 8a shows the wavelength-dependent average visual trans–mittance of untreated and coated (NCL2, NCL5, and NCL7) samples. All coatings show a quick rise in trans–mittance in the UV-visible range (300-500 nm), fol–lowed by a steady response of 21-22% across visible and near-infrared wavelengths. NCL7 has the highest and most uniform transmittance across a large spectral range, while NCL2 exhibits a modest drop in the mid-wavelength area before progressively rebounding. On the other hand, the phase difference Δ in (Figure 8b) quickly decreases with wavelength; higher values for NCL2 and NCL5 reflect stronger UV absorption, while NCL7 exhibits a smoother decay, indicating reduced losses. Overall, these findings demonstrate that Cu–Li co-doping enables precise tuning of the dielectric and optical properties, providing a route to optimize $Li_x Cu_{0.05}Ni_{0.95-x}O$ films for solar energy harvesting, anti-reflective coatings, and other optoelectronic applications.

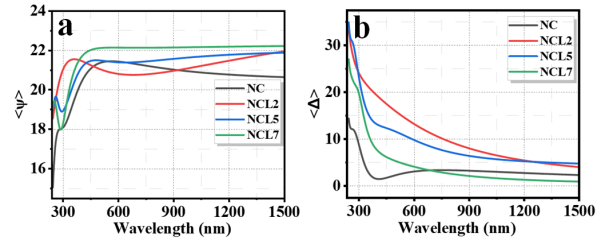



**Figure 8. (a) Psi (ψ) ;(b) Delta (Δ) of $Li_xCu_{0.05}Ni_{0.95-x}O$ films**

The refractive index (n), extinction coefficient, and how the refractive index depends on Li content are shown in Figures 9a, b, and c, respectively. Figure 9a depicts the fluctuation of the refractive index with wavelength for both untreated (NC) and coated samples (NCL2, NCL5, and NCL7). All samples show normal dispersion, with a significant drop in the ultraviolet area (250-400 nm) and gradual stabilization at 1.40-1.50 in the visible and near-infrared regions. Among the coated samples, NCL7 has the lowest refractive index thro–ughout the spectrum, while NCL2 revealed a slightly higher value after 400 nm. The coated films owered and stabilized refractive index indicates better optical properties, making them appropriate for anti-reflective coatings. Moreover, for all the films, there was a sharp decrease in the UV region, followed by a gradual inc–rease in the visible-near IR range, indicating normal dispersion in all the films. Li doping mainly increased the n throughout the whole spectrum, which results in enhanced densification and polarizability of NiO films. The NCL7 sample exhibits the highest n values, indi–cating that Li doping improves electronic interactions and reduces structural defects, thus increasing the optical density of the coating. The extinction coefficient (k) (Figure 9b) shows significant absorption in the UV region, then a steep decline into the visible range. Overall, it was observed that k shows an inverse rela–tionship with Li loading: high Li content results in lower k, especially above 350 nm, indicating fewer electronic defect states and sub-bandgap absorption. The NCL7 film exhibited the lowest k values, indicating better optical transparency and fewer non-radiative recombinations. This reduction in absorption with Li doping is beneficial for developing high-performance optical coatings and low-loss optoelectronic layers.

Figure 9c shows how n varies with Li content at selected measurement wavelengths (400–1200 nm). The maximum increase was observed at x=0.05, followed by a gradual decline, indicating that the optimal Li loading for polarizability and compaction is at x=0.05 [46]. Beyond this concentration, excess Li may agglomerate into phases or disrupt lattice ordering, resulting in a slight reduction in n. The consistent behavior across all wavelengths confirms the strong influence of Li on the optical constants of films. The observed variation in refractive index and extinction coefficient aligns with the changes in crystallinity, grain size, and defect concentration identified by XRD, FESEM, and PL analyses, indicating that Cu–Li co-doping systema–tically alters the electronic structure of NiO.

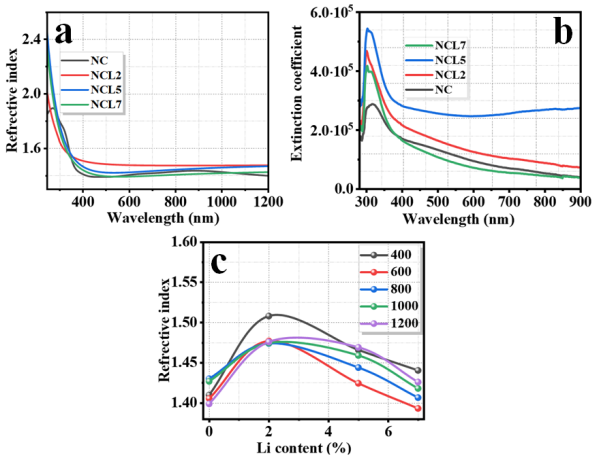



**Figure 9. (a) Refractive index vs. wavelength, (b) Extinction coefficient vs. wavelength, and (c) refractive index with Li content of $Li_xCu_{0.05}Ni_{0.95-x}O$ films.**

Figure 10a presents the room-temperature photolu–minescence spectra of the undoped NC and Li-doped samples. Four emission peaks at 365, 407, 434, and 494

nm are observed and correspond to intrinsic band-edge transitions and defect-related emissions. Li incorpo–ration enhances PL intensity across all emission bands, with NCL7 showing the strongest emission. This enhancement reflects reduced non-radiative recombi–nation, suppression of defect-mediated quenching, and improved activation of radiative centers.

The strong blue emission (407–434 nm) also under–scores the suitability of the films for optoelectronic and visible-light-emissive applications [47]. Figure 10b shows how PL intensities at major emission peaks (365, 407, 434, 494 nm) evolve with increasing Li content. For all emission wavelengths, PL intensity increases monotonically up to 5% Li, after which the intensity slightly decreases. This trend demonstrates an optimal Li concentration that maximizes radiative recombination through defect passivation and improved crystallinity. Beyond this level, excessive Li can introduce new defects or disrupt the local electronic environment, diminishing emission efficiency. The peak enhancement at 5% Li directly correlates with the trends observed in Figure 9c, reinforcing the link between structural qua–lity, optical constants, and luminescent performance [48].

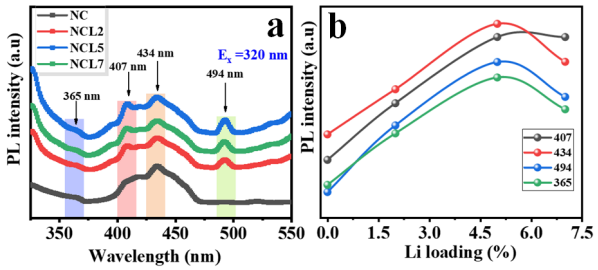



**Figure 10. (a) Photoluminescence (PL) and (b) PL with Li content**

## 4. PRACTICAL APPLICATIONS

The synthesized $Li_xCu_{0.05}Ni_{0.95-x}O$ nanocoatings in this investigation demonstrate promise for advanced trans–parent optoelectronic and sustainable energy appli–cations due to their adjustable structural and optical properties attained by regulated Li–Cu co-doping. These materials are ideal for transparent photovoltaic cells, electrochromic smart windows, thin-film transistors, photodetectors, light-emitting devices, gas sensors, and transparent p-type electrodes due to their optimized crystal structure, tailored bandgap, increased visible-light absorption, and improved dielectric and refractive index properties. Additionally, their superior optical sensitivity and structural stability offer great potential for solar thermal absorber coatings, photo–catalytic reactors, anti-reflective coatings, and protec–tive optical coatings utilized in industrial energy systems.

## 5. CONCLUSIONS

In this work, a systematic study of $Li_xCu_{0.05}Ni_{0.95-x}O$ films was conducted to examine the effect of Li doping within a fixed Cu-doped framework on the optoelec–tronic and structural properties of NiO. The incor–poration of Li preserved the single-phase crystal structure of NiO. However, it consistently increased the lattice parameter and decreased the crystallite size of the NiO film. These structural changes led to a redshift of the absorption edge, a reduction in the band gap at x = 0.07, and a decline in the extinction coefficient across the visible spectrum. Moreover, the ellipsometry analysis confirmed that by adjusting the Li content, the dielectric constants and refractive indices could be tuned, allowing precise control over optical confinement and polarization in NiO films. Additionally, the pho–toluminescence analyses revealed an optimal Li doping level of x=0.05, indicating that at this level, radiative recombination was maximized due to enhanced crys–tallinity and reduced nonradiative losses.

In conclusion, the results demonstrated the syner–gistic effect of co-doping Li and Cu. Li helped to tune the band structure and optical constants, while Cu sta–bilized defect-mediated transitions. This synergistic effect allows the NiO films to customize their refractive index, optical, and luminescent properties traits that are essential for designing next-generation solar cell har–vesting layers, optoelectronic interfaces, and electro–chromic coatings. The demonstrated tunability positions $Li_xCu_{0.05}Ni_{0.95-x}O$ as a versatile materials platform, and the insights gained here can guide future optimization of p-type transparent conducting oxides for high-efficiency device applications.

## 6. LIMITATIONS AND FUTURE WORK

This study shows that Li-Cu co-doping improves the structural and optical properties of $Li_xCu_{0.05}Ni_{0.95-x}O$ nanocoatings. However, it only focuses on material fabrication and physicochemical characterization under laboratory testings. Comprehensive electrical and elec–trochemical characterisation, long-term environmental and thermal stability evaluations, and the commis–sioning of prototype devices to verify optimal per–formance should all be part of future research. Furt–hermore, the optimization of the Cu/Li doping ratio and deposition parameters, as well as integration into transparent photovoltaics, electrochromic devices, and other optoelectronic systems should establish the mate–rial's potential for large-scale industrial and renewable energy applications.


## ACKNOWLEDGMENT

The authors gratefully acknowledge the supprot of Interdisciplinary Research Center for Sustainable Energy Systems (IRC-SES), King Fahd University of Petroleum & Minerals (KFUPM), Saudi Arabia under project grant number INSE2601.


## NOMENCLATURE

| | |
|---|---|
| AOS | Amorphous Oxide Semiconductors |
| DW | Deionized Water |
| EDS | Energy Dispersive X-Ray Spectroscopy |
| FESEM | Field Emission Scanning Electron Microscopy |
| FTIR | Fourier-Transform Infrared |
| FWHM | Full-Width Half Maximum |
| MVB | Maximum Valence-Band |
| MO | Metal Oxide |
| NPs | Nanoparticles |
| NCL | Sample Designation |

| | |
|---|---|
| NIR | Near-Infrared |
| LMNCO | Lithium Manganese Nickel Cobalt Oxide |
| OLED | Organic Light-Emitting Diode |
| PLS | Photoluminescence Spectroscopy |
| SEM | Scanning Electron Microscopy |
| SHIR | Swift Heavy Ion Radiation |
| UV | Ultraviolet |
| UV-Vis | Ultraviolet–Visible Spectroscopy |
| XRD | X-Ray Diffraction |

## REFERENCES


[1] M. Habibi *et al.*, "Intercalation-based electrode materials for lithium-ion batteries: structure, chemistry, and performance," *Chem. Eng. J. Green Sustain.*, vol. 2, p. 100043, Jun. 2026, doi: 10.1016/j.cejgas.2026.100043.

[2] S. Alexander Federovich, K. Sergey Anatolyevich, C. Anatoli Alexandrovich, E. Mikhail Alexandrovich, T. Dragoljub, M. Petro Petrovich, "Application of Chemography Method to Study Surface Damage Phenomena," *FME Trans.*, vol. 50, no. 3, 2022, doi: 10.5937/fme2203484F.

[3] D. W. Davies, C. N. Savory, J. M. Frost, D. O. Scanlon, B. J. Morgan, and A. Walsh, "Descriptors for Electron and Hole Charge Carriers in Metal Oxides," *J. Phys. Chem. Lett.*, vol. 11, no. 2, 2020, doi: 10.1021/acs.jpclett.9b03398.

[4] T. T. Bui, P. Pujar, J.-H. Lee, "Recent advances in 1D metal oxide semiconductor nanofibers for field-effect transistors and emerging applications," *J. Alloys Compd.*, vol. 1078, p. 189762, Jul. 2026, doi: 10.1016/j.jallcom.2026.189762.

[5] T. Kamiya, K. Nomura, H. Hosono, "Origins of High Mobility and Low Operation Voltage of Amorphous Oxide TFTs: Electronic Structure, Electron Transport, Defects and Doping*," *J. Disp. Technol.*, vol. 5, no. 12, 2009, doi: 10.1109/jdt.2009.2034559.

[6] J. Lindahl, J. Keller, O. Donzel-Gargand, P. Szaniawski, M. Edoff, T. Törndahl, "Deposition temperature induced conduction band changes in zinc tin oxide buffer layers for Cu(In,Ga)Se2 solar cells," *Sol. Energy Mater. Sol. Cells*, vol. 144, pp. 684–690, Jan. 2016, doi: 10.1016/j.solmat.2015.09.048.

[7] M. Kimura *et al.*, "Extraction of trap densities in ZnO thin-film transistors and dependence on oxygen partial pressure during sputtering of ZnO films," *IEEE Trans. Electron Devices*, vol. 58, no. 9, 2011, doi: 10.1109/TED.2011.2158546.

[8] Y. Cho *et al.*, "Alkali incorporation into Cu(In,Ga)Se2 determined by crystal orientation of Mo back contact: Implications for highly efficient photovoltaic devices," *Sol. Energy Mater. Sol. Cells*, vol. 188, pp. 46–50, Dec. 2018, doi: 10.1016/j.solmat.2018.08.014.

[9] N. M. Nair, A. Zumeit, R. Dahiya, "Transparent and Transient Flexible Electronics," 2025. doi: 10.1002/advs.202505133.

[10] M. Rahman, "Tin oxide thin films for the future: A paradigm shift in property engineering for advanced functional devices," 2025. doi: 10.1016/j.nxmate.2025.101341.

[11] R. Bintarto, A. Purnowidodo, T. D. Widodo, M. Talice, D. B. Darmadi, "Thermal Insulation Coating Using Natural Stone Powder-Epoxy Composite for Room Temperature Reduction," *FME Trans.*, vol. 51, no. 4, 2023, doi: 10.5937/fme2304457B.

[12] A. Alnassir, F. Albinali, F. Aljaroudi, N. Alsaleem, S. Rehman, "A Comprehensive Review of Existing Erosion Protective Coatings and Practices for Wind Turbine Blade Surfaces," *FME Trans.*, vol. 53, no. 2, 2025, doi: 10.5937/fme2503510A.

[13] M. E. Zayed, "Recent Advances in Solar Thermal Selective Coatings for Solar Power Applications: Technology Categorization, Preparation Methods, and Induced Aging Mechanisms," *Appl. Sci.*, vol. 14, no. 18, p. 8438, Sep. 2024, doi: 10.3390/app14188438.

[14] M. Mrdak, A. Vencl, M. Cosić, "Microstructure and mechanical properties of the Mo-NiCrBSi coating deposited by atmospheric plasma spraying," *FME Trans.*, vol. 37, no. 1, 2009.

[15] S. Petronic, A. Milosavljević, "Heat Treatment Effect on Multicomponent Nickel Alloys Structure," *FME Trans.*, vol. 35, 2007.

[16] N. S. Das, B. Saha, R. Thapa, G. C. Das, K. K. Chattopadhyay, "Band gap widening of nanocrystalline nickel oxide thin films via phosphorus doping," *Phys. E Low-Dimensional Syst. Nanostructures*, vol. 42, no. 5, 2010, doi: 10.1016/j.physe.2009.11.047.

[17] Y. Lee, T. G. Hwang, W. J. Cho, K. J. Lee, H. Park, "Solution-processed cobalt doping for performance enhancement of p-type NiO thin-film transistors," *Micro and Nanostructures*, vol. 205, 2025, doi: 10.1016/j.micrna.2025.208196.

[18] M. E. Zayed, A. H. Elsheikh, F. A. Essa, A. M. Elbanna, W. Li, J. Zhao, "High-temperature solar selective absorbing coatings for concentrated solar power systems," in *Sustainable Materials and Green Processing for Energy Conversion*, 2022. doi: 10.1016/B978-0-12-822838-8.00010-7.

[19] R. C. Boutwell, M. Wei, A. Scheurer, J. W. Mares, W. V. Schoenfeld, "Optical and structural properties of NiMgO thin films formed by sol-gel spin coating," *Thin Solid Films*, vol. 520, no. 13, 2012, doi: 10.1016/j.tsf.2012.02.065.

[20] J. D. Castro *et al.*, "Morphological and structural analysis of gradient Ni and Mn-doped lithium cobalt oxide thin films for lithium-ion battery applications," *Thin Solid Films*, vol. 837, p. 140888, Mar. 2026, doi: 10.1016/j.tsf.2026.140888.

[21] M. R. Hosseinzade, L. Naji, F. Hasannezhad, "Electrochemical synthesis of Cu-doped nickel oxide thin film on indium tin oxide as hole transport layer in polymer solar cells," *Mater. Sci. Semicond. Process.*, vol. 199, 2025, doi: 10.1016/j.mssp.2025.109885.

[22] Karishma, A. Tripathi, V. Bhushan, V. Sharma, "60 MeV Si ion beam irradiation induced modifications

in the structural and optical properties of Li doped NiO thin films," in *Materials Today: Proceedings*, 2023. doi: 10.1016/j.matpr.2023.01.020.

[23] Q. Huang, Q. Zhang, Y. Xiao, Y. He, X. Diao, "Improved electrochromic performance of NiO-based thin films by lithium and tantalum co-doping," *J. Alloys Compd.*, vol. 747, 2018, doi: 10.1016/j.jallcom.2018.02.232.

[24] F. Lin *et al.*, "Electrochromic performance of nanocomposite nickel oxide counter electrodes containing lithium and zirconium," *Sol. Energy Mater. Sol. Cells*, vol. 126, 2014, doi: 10.1016/j.solmat.2013.11.023.

[25] [25] D. Gillaspie, A. Norman, C. E. Tracy, J. R. Pitts, S.-H. Lee, A. Dillon, "Nanocomposite Counter Electrode Materials for Electrochromic Windows," *J. Electrochem. Soc.*, vol. 157, no. 3, 2010, doi: 10.1149/1.3276779.

[26] X. Chen, L. Zhao, and Q. Niu, "Electrical and optical properties of p-type Li,Cu-codoped NiO thin films," *J. Electron. Mater.*, vol. 41, no. 12, 2012, doi: 10.1007/s11664-012-2213-4.

[27] B. Uzunbayır, S. A. Akalın, S. Yıldırım, M. Erol, and S. Oğuzlar, "Production and Characterizations of Sol–Gel-Derived Li, Cu:NiOx Particles: An Investigation on the Effects of Li and Cu Incorporation," *J. Electron. Mater.*, vol. 52, no. 8, 2023, doi: 10.1007/s11664-023-10500-z.

[28] J. Y. Zhang *et al.*, "Electronic and transport properties of Li-doped NiO epitaxial thin films," *J. Mater. Chem. C*, vol. 6, no. 9, 2018, doi: 10.1039/c7tc05331b.

[29] K. Sheshadri, D. Malterre, A. Fujimori, A. Chainani, "Connecting the one-band and three-band Hubbard models of cuprates via spectroscopy and scattering experiments," *Phys. Rev. B*, vol. 107, no. 8, 2023, doi: 10.1103/PhysRevB.107.085125.

[30] A. S. Bhatt *et al.*, "Optical and electrochemical applications of Li-doped NiO nanostructures synthesized via facile microwave technique," *Materials (Basel).*, vol. 13, no. 13, 2020, doi: 10.3390/ma13132961.

[31] J. Y. Chang, Y. C. Chen, C. M. Wang, Y. W. Chen, "electrochromic properties of Li-Doped NiO films prepared by RF magnetron sputtering," *Coatings*, vol. 10, no. 1, 2020, doi: 10.3390/coatings1001 0087.

[32] W. Chen *et al.*, "Understanding the Doping Effect on NiO: Toward High-Performance Inverted Perovskite Solar Cells," *Adv. Energy Mater.*, vol. 8, no. 19, 2018, doi: 10.1002/aenm.201703519.

[33] Z. He, Z. Ji, S. Zhao, C. Wang, K. Liu, Z. Ye, "Characterization and electrochromic properties of CuxNi 1-xO films prepared by sol-gel dip-coating," in *Solar Energy*, 2006. doi: 10.1016/j.solener.2005.02.007.

[34] Q. He, K. Yao, X. Wang, X. Xia, S. Leng, and F. Li, "Room-Temperature and Solution-Processable Cu-Doped Nickel Oxide Nanoparticles for Efficient Hole-Transport Layers of Flexible Large-Area Perovskite Solar Cells," *ACS Appl. Mater. Interfaces*, vol. 9, no. 48, 2017, doi: 10.1021/acsami.7b13621.

[35] Y. Wang, T. Mahmoudi, Y. B. Hahn, "Highly stable and Efficient Perovskite Solar Cells Based on FAMA-Perovskite-Cu:NiO Composites with 20.7% Efficiency and 80.5% Fill Factor," *Adv. Energy Mater.*, vol. 10, no. 27, 2020, doi: 10.1002/aenm.202000967.

[36] [36] K. Varunkumar, R. Hussain, G. Hegde, A. S. Ethiraj, "Effect of calcination temperature on Cu doped NiO nanoparticles prepared via wet-chemical method: Structural, optical and morphological studies," *Mater. Sci. Semicond. Process.*, vol. 66, 2017, doi: 10.1016/j.mssp.2017.04.009.

[37] S. A. Mahmoud, A. A. Akl, H. Kamal, K. Abdel-Hady, "Opto-structural, electrical and electrochromic properties of crystalline nickel oxide thin films prepared by spray pyrolysis," *Phys. B Condens. Matter*, vol. 311, no. 3–4, 2002, doi: 10.1016/S0921-4526(01)01024-9.

[38] B. Huo, S. Peng, T. Wang, D. Deng, X. Yan, L. Luo, "Heterojunction NiO/CuO hollow nanospheres: Enhanced electronic conductivity and specific surface area for electrochemical determination of glucose," *J. Electroanal. Chem.*, vol. 1013, p. 120131, Jul. 2026, doi: 10.1016/j.jelechem.2026.120131.

[39] M. Aftab, M. Z. Butt, D. Ali, F. Bashir, T. M. Khan, "Optical and electrical properties of NiO and Cu-doped NiO thin films synthesized by spray pyrolysis," *Opt. Mater. (Amst).*, vol. 119, 2021, doi: 10.1016/j.optmat.2021.111369.

[40] Y. E. Firat, A. Peksoz, "Efficiency enhancement of electrochromic performance in NiO thin film via Cu doping for energy-saving potential," *Electrochim. Acta*, vol. 295, 2019, doi: 10.1016/j.electacta.2018.10.166.

[41] A. Sawaby, M. S. Selim, S. Y. Marzouk, M. A. Mostafa, A. Hosny, "Structure, optical and electrochromic properties of NiO thin films," *Phys. B Condens. Matter*, vol. 405, no. 16, pp. 3412–3420, Aug. 2010, doi: 10.1016/j.physb.2010.05.015.

[42] Q. Hu *et al.*, "Hollow Cu-doped NiO microspheres as anode materials with enhanced lithium storage performance," *RSC Adv.*, vol. 9, no. 36, 2019, doi: 10.1039/c9ra03780b.

[43] M. Dinulović, B. Rašuo, "Dielectric properties modeling of composite materials," *FME Trans.*, vol. 37, no. 3, 2009.

[44] M. Dinulović, B. Rašuo, "IEEE," *Compos. Struct.*, vol. 93, no. 12, pp. 3209–3215, Nov. 2011, doi: 10.1016/j.compstruct.2011.05.036.

[45] M. Al-Rasheidi, F. Khan, A. Al-Ahmed, S. Rehman, F. Al-Sulaiman, "Cd-doped ZnO-based electron transport layer for organic-inorganic hybrid perovskite cells: Experimental and numerical study," *Opt. Mater. (Amst).*, vol. 126, 2022, doi: 10.1016/j.optmat.2022.112144.

[46] Z. El Khalidi, S. Fadili, B. Hartiti, A. Lfakir, P. Thevenin, and M. Siadat, "Behavior of NiO thin

films sprayed at different annealing time," *Opt. Quantum Electron.*, vol. 48, no. 9, 2016, doi: 10.1007/s11082-016-0694-8.

[47] L. Zhao *et al.*, "Field-Effect Control in Hole Trans–port Layer Composed of Li:NiO/NiO for Highly Efficient Inverted Planar Perovskite Solar Cells," *Adv. Mater. Interfaces*, vol. 9, no. 2, 2022, doi: 10.1002/admi.202101562.

[48] Z. Yang *et al.*, "Research on the influence of the morphology and crystal structure of NiO and Cu-NiO nanofilms on nonlinear absorption properties in the visible light band," *J. Alloys Compd.*, vol. 1032, 2025, doi: 10.1016/j.jallcom.2025.180878.

## ИНЖЕЊЕРИНГ СТРУКТУРНИХ СВОЈСТАВА И ЕНЕРГЕТСКОГ ПРОЦЕПА NiO НАНОСТРУКТУРА КО-ДОПИРАНИХ БАКРОМ И ЛИТИЈУМОМ ЗА ПРИМЕНЕ У ОПТОЕЛЕКТРОНИЦИ И ЕНЕРГЕТИЦИ

**Ш. Риаз, С. Камран, М. А-Рашиди, М.Е. Зајед, Ш. Рехман, Ф. Кан**

Ова студија представља наноструктуре никл-оксида (NiO) ко-допиране бакром (Cu) и литијумом (Li), које показују значајна побољшања структурних и оптичких својстава. Узорци NiO – укључујући чисти NiO, као и верзије допиране једним елементом или ко-допиране – синтетисани су хидротермалном ме–тодом. Структурне, оптичке и морфолошке карак–теристике анализиране су помоћу дифракције X-зрака (XRD), UV-видљиве спектроскопије и скени–рајуће електронске микроскопије (SEM). Резултати XRD анализе открили су побољшану кристалност NiO филмова услед двоструког допирања, што ове материјале чини перспективним за примене у микроелектроници. Индекс преламања и коефи–цијент апсорпције показали су побољшања код NiO узорака, како при једноструком, тако и при ко-допирању. Енергија енергетског процепа смањила се са 3,50 eV код NiO допираног бакром на 3,34 eV код филмова ко-допираних бакром и литијумом. Ово смањење енергетског процепа указује на то да ко-допирање бакром и литијумом значајно побољшава електрохромне карактеристике NiO узорака. Пове–ћана апсорбанција код узорка NCL7 истиче потен–цијал за прецизно подешавање нивоа допаната ради даљег побољшања перформанси.